ISA Transactions 52 (2013) 358–364

Contents lists available at SciVerse ScienceDirect

ISA Transactions

journal homepage: www.elsevier.com/locate/isatrans

Research Article

Modeling and simulation of soft sensor design for real-time speed estimation, measurement and control of induction motor

Erik Etien*

LIAS (Laboratory of Informatic and Automatic for the Systems), University of Poitiers, Bâtiment B25 - 2, rue Pierre Brousse BP 633 86022 Poitiers Cedex, France

ARTICLE INFO

Article history:
Received 10 June 2012
Received in revised form
12 November 2012
Accepted 13 November 2012
Available online 17 January 2013
This paper was recommended for publication by Dr. A.B. Rad.

Keywords:
Design
Modeling
Simulation
Motor speed control
Soft sensor
Stability analysis

ABSTRACT

This paper deals with the design of a speed soft sensor for induction motor. The sensor is based on the physical model of the motor. Because the validation step highlight the fact that the sensor cannot be validated for all the operating points, the model is modified in order to obtain a fully validated sensor in the whole speed range. An original feature of the proposed approach is that the modified model is derived from stability analysis using automatic control theory.

1. Introduction

Soft sensors are a valuable tools in many different industrial fields of application. They are used to solve a number of problems such as measuring system back-up, what-if analysis, real-time prediction for plant control, sensor validation and fault diagnosis strategies. In electrical motors drives, soft sensors offer a number of attractive properties as one of which is a low cost alternative to hardware speed measurement used in classical motor drives [1–3]. For a long time, soft sensors have been based on physical models and derived from methods inspired from control theory [4–6], such as adaptive observers [7–9], reference models [10–12]. Whatever the chosen method, the sensor design procedure is summarized in Fig. 1 [13].

In electrical motor drives, data selection is limited to measured signals, i.e. stator currents. Stator voltages can be measured, but due to economical constraints, actual voltages are replaced by estimated ones stemmed from control. In this paper, limiting measurements to stator currents is motivated by the desire to be close to the operating conditions of industrial drives. In main applications, the physical motor model is used in order to design the control and to estimate unmeasured signals (Section 2). Appropriate assumptions allow to neglect nonlinear effects as saturations, iron losses or magnetic hysteresis in order to derive a simplified physical model. It yields a good approximation of the motor behavior which is sufficient for control objectives. The identification step concerns the determination of model parameters. Several strategies can be considered for this identification during functioning or before functioning, at zero speed or using specifical tests offline [14]. In Section 3, an identification procedure using a Levenberg–Marquardt algorithm is presented. The final step towards the identification is the validation. This phase requires us to verify whether the model is able to adequately represent the system. In this case, the data which are used for validation should be different from those used for model identification. In this article, a stability study, based on automatic control theory is used in order to validate the proposed model (Section 4). If the validation test fails, the soft sensor design should be reconsidered. In Section 5, we show how the validation procedure can lead to a model modification (Fig. 1).

2. Model selection

2.1. Motor model

Fig. 2 shows the three-phase representation of the induction motor (IM). The stator and the rotor are usually modeled as three windings 120° spatially displaced. It is well-known that the manipulation of the three-phase model is not easy. Under particular assumptions, this model can be reduced to a two-phase

* Tel.: +33 549453509; fax: +33 549454034.
E-mail address: erik.etien@univ-poitiers.fr

0019-0578/$ - see front matter © 2012 ISA. Published by Elsevier Ltd. All rights reserved.
http://dx.doi.org/10.1016/j.isatra.2012.11.001

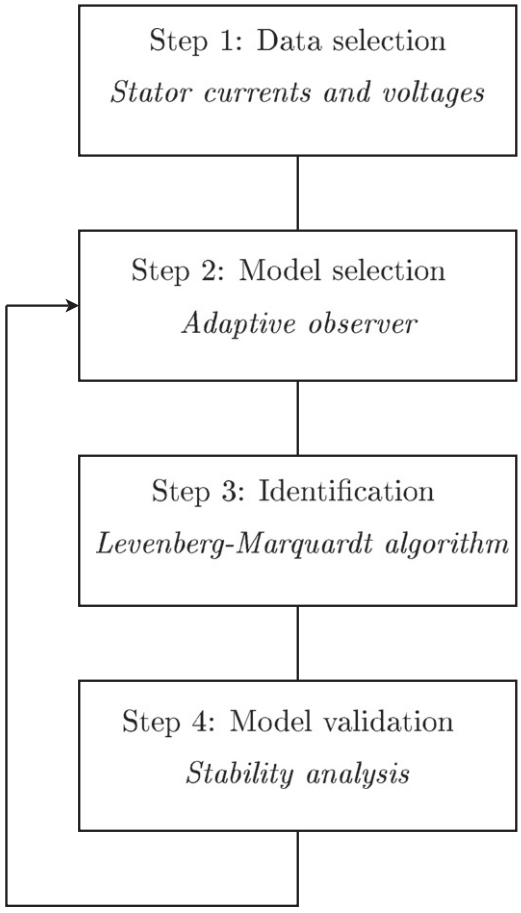

Fig. 1. Soft sensor development.

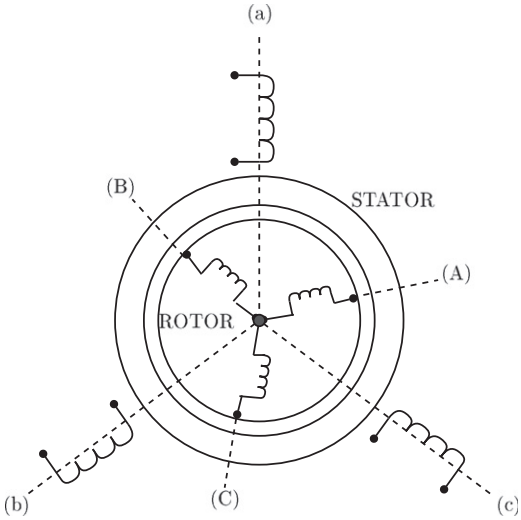

Fig. 2. Induction motor representation in three-phase co-ordinate.

one [15]. As a consequence, three-phase electrical quantities (stator currents, stator voltages, rotor flux…) can be reduced to vectors (named phasors) which co-ordinates are expressed in different reference frames. Fig. 3 shows a representation of the stator current phasor $\underline{i}_s$ in one hand in a fixed reference frame $\{\alpha, \beta\}$ $(\theta_g = 0)$ and in other hand in a rotating reference frame $\{d,q\}$. In the fixed reference frame, three-phase sinusoidal signals are reduced to two-phase sinusoidal ones. In the rotating reference frame, the two-phase signals can be made continuous if the

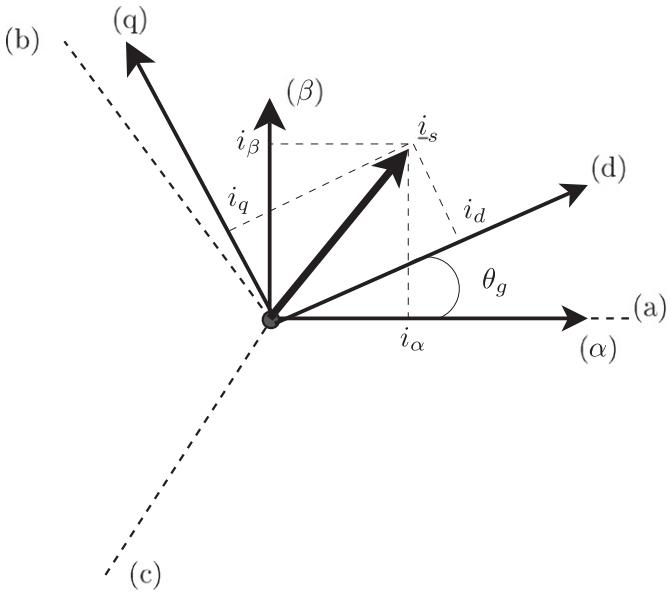

Fig. 3. Stator current vector representation in two phase references ($\{\alpha, \beta\}$ and $\{d,q\}$).

rotation frequency of the frame $(\omega_g = \dot{\theta}_g)$ is equal to the electrical supply frequency (ω_s). This choice is particularly suitable when electrical quantities must be controlled.

According to previous considerations, the general induction motor model, expressed in an arbitrary reference frame rotating at frequency ω_g, is given by

$$\begin{cases} \dfrac{d}{dt}\underline{i}_s = -\left(\dfrac{1}{\tau_\sigma} + j\omega_g\right)\underline{i}_s + \dfrac{1}{L_\sigma}\left(\dfrac{1}{\tau_R} - j\omega\right)\underline{\psi}_R + \dfrac{1}{L_\sigma}\underline{u}_s, \\ \dfrac{d}{dt}\underline{\psi}_R = R_R\underline{i}_s - \left(\dfrac{1}{\tau_R} + j(\omega_g - \omega)\right)\underline{\psi}_R, \\ \dfrac{J}{P}\dfrac{d}{dt}\omega = T_{em} - T_L - f\omega, \\ T_{em} = \dfrac{3}{2}P(\psi_{Rd}i_{sq} - \psi_{Rq}i_{sd}) \end{cases} \tag{1}$$

with $\underline{i}_s = i_{sd} + ji_{sq}$, $\underline{\psi}_R = \psi_{Rd} + j\psi_{Rq}$, $\underline{u}_s = u_{sd} + ju_{sq}$. Time constants are defined by $\tau_\sigma = L_\sigma/(R_s + R_R)$, $\tau_R = L_M/R_R$. The four motor parameters are R_s, stator resistance; R_R, the rotor resistance; L_σ, stator transient inductance; L_M, magnetizing inductance and P, the number of poles pairs. On the one hand, the electrical rotor frequency, ω (in rad/s), is related to the electric supply frequency (ω_s) by $\omega_s = \omega + \omega_{sl}$, where ω_{sl} is the slip frequency. On the other hand, the relationship between ω and the mechanical frequency Ω is $\omega = P\Omega$, and the rotational speed of the motor is $N = 30\Omega/\pi$ (in rpm). T_{em} is the electromagnetic torque produced by the motor and T_L is the torque applied to the motor by its load.

The corresponding motor model expressed in the fixed reference $(\omega_g = 0)$ frame can be expressed by

$$\begin{cases} \dfrac{d}{dt}\underline{X} = A\underline{X} + B\underline{U} = \begin{pmatrix} A_{11} & A_{12} \\ A_{21} & A_{22} \end{pmatrix}\underline{X} + \begin{bmatrix} B_1 \\ B_2 \end{bmatrix}\underline{U}_s, \\ \underline{Y} = \underline{I}_s = C\underline{X} \end{cases} \tag{2}$$

with $\underline{X} = \begin{bmatrix} \underline{I}_s \\ \underline{\Psi}_R \end{bmatrix}$ where $\underline{I}_s(t) = \begin{bmatrix} i_{s\alpha} \\ i_{s\beta} \end{bmatrix}$ and $\underline{\Psi}_R(t) = \begin{bmatrix} \psi_{R\alpha} \\ \psi_{R\beta} \end{bmatrix}$. The input vector is $\underline{U}_s(t) = \begin{bmatrix} u_{s\alpha} \\ u_{s\beta} \end{bmatrix}$. The involved matrices are defined by

$$A_{11} = \begin{pmatrix} -\dfrac{1}{\tau_\sigma} & 0 \\ 0 & -\dfrac{1}{\tau^\sigma} \end{pmatrix}, \quad A_{12} = \begin{pmatrix} \dfrac{1}{\tau_R L_\sigma} & \dfrac{\omega}{L_\sigma} \\ \dfrac{-\omega}{L_\sigma} & \dfrac{1}{\tau_R L_\sigma} \end{pmatrix},$$

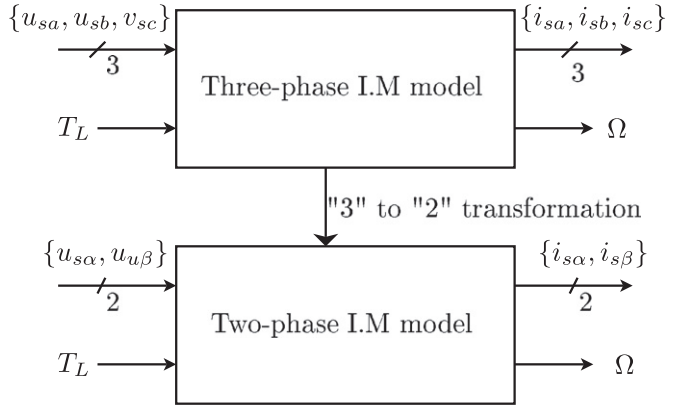

Fig. 4. Dimension reduction of the induction motor model.

$$A_{21} = \begin{pmatrix} R_R & 0 \\ 0 & R_R \end{pmatrix}, \quad A_{22} = \begin{pmatrix} -\frac{1}{\tau_R} & -\omega \\ \omega & -\frac{1}{\tau_R} \end{pmatrix},$$

$$B_1 = \begin{pmatrix} \frac{1}{L_\sigma} & 0 \\ 0 & \frac{1}{L_\sigma} \end{pmatrix}, \quad B_2 = \begin{pmatrix} 0 & 0 \\ 0 & 0 \end{pmatrix},$$

$$C = \begin{pmatrix} 1 & 0 & 0 & 0 \\ 0 & 1 & 0 & 0 \end{pmatrix}.$$

Fig. 4 shows the reduced model obtained by the three-phase to the two-phase transformation in the fixed reference frame named Concordia transform. After transformation, the model inputs are the stator voltages $\{u_{s\alpha}, u_{s\beta}\}$ applied the motor and the load torque T_L imposed by the load. The model outputs are the stator currents $\{i_{s\alpha}, i_{s\beta}\}$ and the rotor mechanical frequency Ω.

A natural approach to design a soft sensor which can measure the mechanical speed Ω would be to simulate Eq. (1). In practical applications, input voltages and output currents are measured in the three-phase frame and transposed in the fixed reference frame. Internal variables $\{\psi_{R_\alpha}, \psi_{R_\beta}\}$ are not measurable and are simulated using Eq. (2) based on the knowledge of electrical motor parameters. The mechanical frequency ω (and consequently Ω) cannot be obtained from Eq. (1) because, without torque sensor, the load torque T_L is unknown. In order to derive a soft sensor measuring Ω, this equation must be replaced by another one which expresses as well as possible the mechanical behavior of the motor. This equation is named adaptation law and must guarantee a correct estimation of the frequency Ω for all the operating points of the motor. If this goal is reached, the speed soft sensor can be considered as validated.

2.2. Sensor model

2.2.1. Model description

The first part of the sensor model is built using Eq. (2) and assuming that electrical parameters are known:

$$\begin{cases} \frac{d}{dt}\underline{\widehat{X}} = \underbrace{\begin{pmatrix} A_{11} & \widehat{A}_{12} \\ A_{21} & \widehat{A}_{22} \end{pmatrix}}_{\widehat{A}} \underline{\widehat{X}} + \begin{bmatrix} B_1 \\ B_2 \end{bmatrix} \underline{U_s} + G\underline{E_i}, \\ \underline{\widehat{I}_s} = C\underline{\widehat{X}} \end{cases} \tag{3}$$

with $\underline{E_i} = \underline{I_s} - \underline{\widehat{I}_s}$ and

$$\widehat{A}_{12} = \begin{pmatrix} \frac{1}{\tau_R L_\sigma} & \frac{\widehat{\omega}}{L_\sigma} \\ \frac{-\widehat{\omega}}{L_\sigma} & \frac{1}{\tau_R L_\sigma} \end{pmatrix}, \quad \widehat{A}_{22} = \begin{pmatrix} -\frac{1}{\tau_R} & -\widehat{\omega} \\ \widehat{\omega} & -\frac{1}{\tau_R} \end{pmatrix}.$$

Superscript "^" denotes estimated variables. In comparison with (2), a correction term is added through the gain matrix $G = \begin{bmatrix} G_s \\ G_r \end{bmatrix}$. Considering $G=0$, the model (3) is a strict simulation of the motor equations with $\underline{U_s}$ as input signal. Better performances can be achieved using stator currents $\underline{I_s}$ as second input through feedback gains G_s and G_r. Moreover, as shown in the remainder of the paper, the gain G can be designed to obtain a complete validation of the soft sensor.

The soft sensor also consists of the electrical frequency estimation $\widehat{\omega}$ by means of an adaptation law. This adaptive law can exploit all the available measures; it can be expressed as

$$\widehat{\omega} = f(\underline{I_s}, \underline{\widehat{I}_s}, \underline{\widehat{\Psi}_R}). \tag{4}$$

The complete soft sensor is shown in Fig. 5.

In order to complete the sensor model selection, the adaptation law (4) must be designed to guarantee that the sensor provides a suitable electrical frequency estimation for all the operating points of the motor. It can be checked by proving that $\underline{E_i} \to 0$ for all the operating points considered. In [7], the authors use the Lyapunov theory in order to find the following adaptation law:

$$\frac{d\widehat{\omega}}{dt} = \frac{\lambda}{L_\sigma}[e_{i_{s\alpha}} \widehat{\psi}_{R_\beta} - e_{i_{s\beta}} \widehat{\psi}_{R_\alpha}] = -K_i \epsilon \tag{5}$$

with $e_{i_{s\alpha}} = i_{s\alpha} - \widehat{i}_{s\alpha}$ and $e_{i_{s\beta}} = i_{s\beta} - \widehat{i}_{s\beta}$.

3. Identification

The parameter vector is defined by $\widehat{\theta} = [\widehat{L}_\sigma \ \widehat{R}_R \ \widehat{R}_s \ \widehat{L}_M]^T$ [16]. It is estimated by minimizing the following criterion:

$$J = \underline{\epsilon}^T \underline{\epsilon} = \sum_{k=1}^{K} ((i_{sdk} - \widehat{i}_{sdk})^2 + (i_{sqk} - \widehat{i}_{sqk})^2), \tag{6}$$

where $\underline{\epsilon}$ is the residual vector which belongs to $\Re^{K\times 1}$ (K is the number of samples). The criterion J is a scalar which represents the sum of the quadratic errors between measured and estimated outputs [17]. Optimal values are obtained using the iterative Levenberg–Marquardt algorithm [18] which achieves a compromise between the stability of the Gradient method and the rapid convergence rate of the Gauss–Newton method:

$$\underline{\hat{\theta}}_{j+1} = \underline{\hat{\theta}}_j - [J'' + \lambda I)^{-1} J']_{\underline{\hat{\theta}} = \underline{\hat{\theta}}_j}. \tag{7}$$

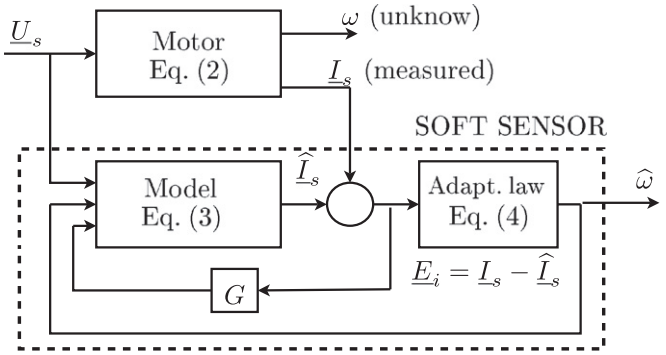

Fig. 5. Block diagram of the soft sensor.

The parameter λ is tuned during the procedure. Thus, this algorithm oscillates between the gradient ($\lambda \gg 1$) and the Newton ($\lambda \ll 1$) methods.

The pseudo-Hessian J'' and the gradient J' can be written as

$$J' = \frac{\partial J}{\partial \underline{\hat{\theta}}} = -2\underline{\epsilon}^T \sigma_{\underline{\hat{\theta}}}, \tag{8}$$

$$J'' = \frac{\partial^2 J}{\partial \underline{\hat{\theta}}^2} \cong 2\sigma_{\underline{\hat{\theta}}}^T \sigma_{\underline{\hat{\theta}}}, \tag{9}$$

where $\sigma_{\underline{\hat{\theta}}} \in \Re^{K\times 4}$ is the sensitivity function matrix defined by

$$\sigma_{\underline{\hat{\theta}}} = \frac{\partial \underline{\hat{Y}}}{\partial \underline{\hat{\theta}}} = \left[\frac{\partial \underline{\hat{Y}}}{\partial \hat{L}_\sigma} \quad \frac{\partial \underline{\hat{Y}}}{\partial \hat{R}_R} \quad \frac{\partial \underline{\hat{Y}}}{\partial \hat{R}_s} \quad \frac{\partial \underline{\hat{Y}}}{\partial \hat{L}_M}\right] \tag{10}$$

with $\underline{\hat{Y}}$ the vector of estimated outputs.

The sensitivity functions quantify the dependence of the model predictions with respect to the parameters. The Euler approximation may be used to calculate these derivatives, considering small variations $\epsilon\underline{\hat{\theta}}$ around the parameter vector $\underline{\hat{\theta}}$:

$$\sigma_{\underline{\hat{\theta}}} = \frac{\underline{\hat{Y}}(\underline{\hat{\theta}}(1+\epsilon)) - \underline{\hat{Y}}(\underline{\hat{\theta}})}{\epsilon\underline{\hat{\theta}}}. \tag{11}$$

The identification procedure is tested on a 1.1-kW four-pole induction motor with nominal speed $N=1470$ rpm and rated torque $T_L=7$ N m. The motor is fed by a frequency converter controlled by a dSpace DS1104 Controller Board. The real-time hardware based on PowerPC technology and its set of I/O interfaces are controlled with Matlab (2007b, 7.5.0) and simulink (RTI 6.2). The load torque is provided by an DC motor (D.C.M) fed by a frequency converter and for the identification, the rotor speed is measured.

In Table 1, estimated electrical parameters, provided by the identification procedure are given for different loads.

Using these parameters, the soft sensor can be implemented in order to measure the rotor speed. The complete set of parameters is given in Table 2.

In the following part, one shows that the model cannot be validated for all the operating points leading to a model modification.

Table 1
Estimated parameters for different loads.

Load (%)	R_s	R_R	L_σ	L_M
30	10.75	3.56	0.06	0.42
50	10.85	361	0.06	0.42
70	10.95	3.65	0.06	0.42
100	11	3.68	0.05	0.42

Table 2
Parameters of 1.1-kW four-pole 400-V 50-Hz motor and load.

Stator resistance, R_s	11 Ω
Rotor resistance, R_R	3.62 Ω
Magnetizing inductance, L_M	420 mH
Leakage inductance, L_σ	60 mH
Total moment of inertia	0.040 kg m^2
Rated speed	1470 r/mn
Rated current	2.6 A
Rated torque	7 N m

4. Model validation

4.1. Simulations

In order to be validated, the soft sensor must provide good speed measurements for all the operating points of the motor. Each operating point is defined by the pair $\{\Omega_0, T_{L0}\}$ (index 0 indicates steady state operation). The induction motor is driven through a Field Oriented Control (FOC) with a model expressed in synchronous reference frame ($\omega_g = \omega_s$). The speed controller imposes the rotor speed ($\Omega = \Omega_{REF}$) whatever the load torque (T_L) is provided by the D.C motor. Current controllers allow the designer to control, on the one hand, the rotor flux through the current $i_{sd} = i_{sdREF}$ and on the other hand, the electromagnetic torque T_{em} through the current $i_{sq} = i_{sqREF}$ (Fig. 7).

The control system is simulated with Matlab/Simulink. Several tests can be performed to investigate the sensor validation; among them, reversal speed at nominal torque and slow load variations at constant speed are particularly used since they

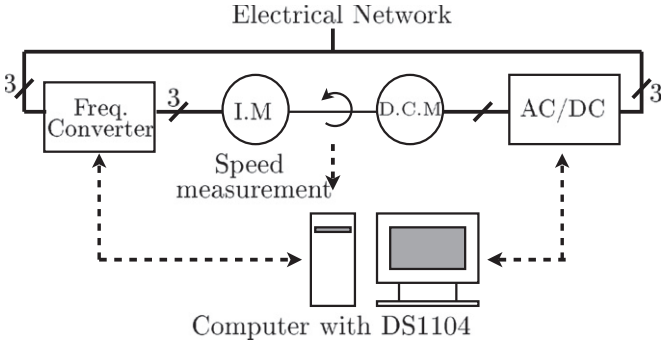

Fig. 6. Experimental setup.

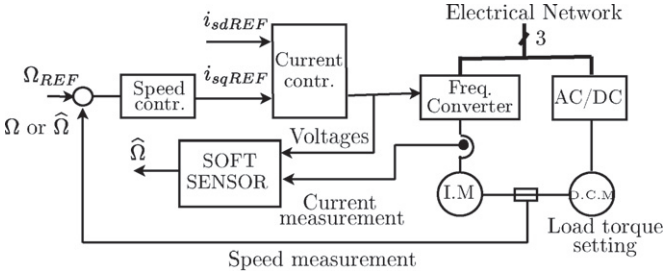

Fig. 7. Block diagram of the control system.

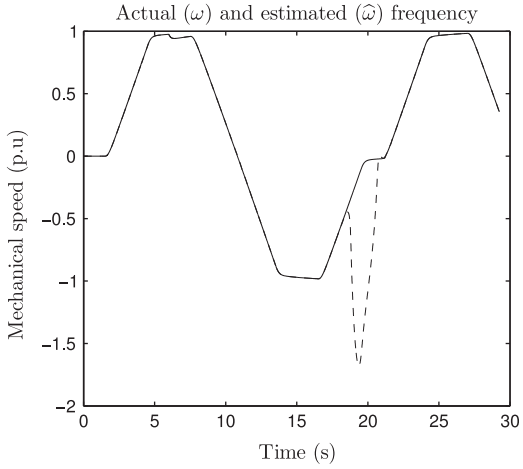

Fig. 8. Simulations: reversal test. Speed varies from 1 p.u. to −1 p.u under nominal torque, $K_i=100$, $G=0$. Actual speed (solid line), estimated speed (dashed line).

correspond to realistic cases. Fig. 8 shows simulation results obtained at the nominal load torque. The speed reference reverses from 1 p.u. to −1 p.u. and the nominal load torque (1 p.u) is applied at $t=6$ s. (The p.u representation is obtained by dividing the measured signal by its nominal value.) It can be shown that the soft sensor does not provide correct estimation in the whole speed range at nominal torque. In particular, the model diverges from real value at low speed around 0.

In order to investigate the influence of the load torque value on the validity domain, a test at slow load variations and constant speed can be used. In this case, the speed reference is held constant and the load torque is increased slowly from 0 to its nominal value. Fig. 9 shows results plotted in the plan $\{\omega, T_L\}$. The sensor works correctly except at low speed, in the regenerating mode defined by $\omega \times T_L < 0$.

The control system is implemented in the experimental plant shown in Fig. 6. Results are presented in Figs. 10 and 11. As expected, it can be verified that the sensor is not validated in regenerating mode for low speed [19,20].

According to previous results, two questions must be investigated:

- Is it possible to analytically determine the validity range?

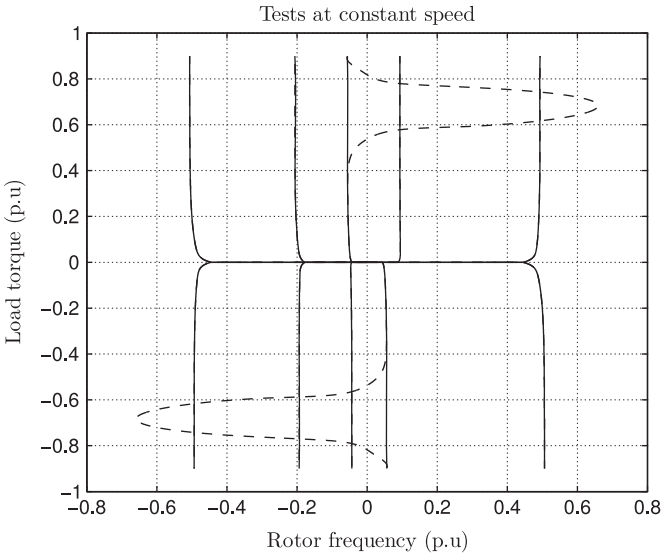

Fig. 9. Simulations: tests at constant speed. Load torque varies from 0 p.u. to 1 p.u and 0 p.u. to −1 p.u, $K_i=100$, $G=0$. Actual speed (solid line), estimated speed (dashed line).

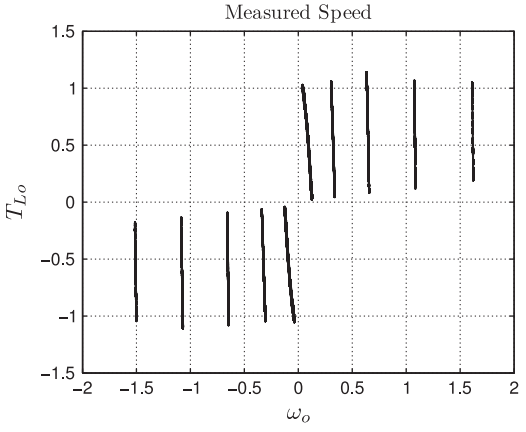

Fig. 10. Experimental results: test in motoring mode in the $\{\omega_0, T_{L0}\}$ plane, $K_i=1$, $K_p=0$, $G_s=G_r=0$. Rotor speed kept constant: $\omega_0=-0.05,-0.2,-0.6,-1,-1.5$ (quadrant 3), $\omega_0=+0.05,+0.2,+0.6,+1,+1.5$ (quadrant 1). Ramp of load torque from 0 to 1 (quadrant 1), from 0 to −1 (quadrant 3) during 100 s. Actual and estimated speeds are superimposed.

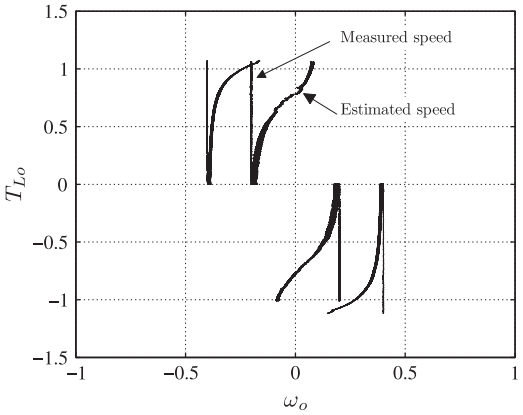

Fig. 11. Experimental results: test in regenerating mode in the $\{\omega_0, T_{L0}\}$ plane, $K_i=1$, $K_p=0$, $G_s=G_r=0$. Rotor speed kept constant: $\omega_0=-0.2$ and $\omega_0=-0.4$ (quadrant 2), $\omega_0=+0.2$ and $\omega_0=+0.4$ (quadrant 4). Ramp of load torque from 0 to 1 (quadrant 2), from 0 to −1.5 (quadrant 4) during 100 s.

- What is the model modification which leads to a validated sensor in the whole speed range?

4.2. Determining the limits of validity

Results of Section 4.1 show that outside of the validity domain, the estimated speed diverges from real one. It can be interpreted as a stability problem meaning that, in this region the system (3) is unstable. As a consequence, a stability study can provide clear indications about the stability range. In general, methods used to study this stability are based on Routh–Hurwitz criterion applied to a transfer function representation [21,22]. These methods can lead to good results but are suitable for SISO systems. In the case of multi-variable models, these approaches quickly become complicated. Moreover, each solution seems to be a particular case and no general analysis is discussed. In [23], a common framework based on the positive-real property is proposed but is not really appropriate to sensor design objectives. In this paper, the stability problem is tackled using a state representation and a very simple criterion is defined, leading to a simplified analysis.

In [24], the authors propose a general framework in order to study the stability of speed estimators for induction motors. An error system is defined by subtracting Eqs. (2) and (3). By linearizing the resulting system $(\underline{e}=\underline{e}_0+\delta\underline{e})$ a linearized model is derived. The stability can be studied by calculating unstable eigenvalues (UEV) and unstable areas are highlighted by plotting UEV in the torque/speed plane. As on the illustration, let us consider the induction motor whose parameters are shown in Table 2. For the classical observer corresponding to the particular case $G_s=G_r=0$, [7] and $K_i=30$, UEV are calculated and plotted in Fig. 12. As expected, the motor model is unstable in regenerating mode at low speed. In this area the soft sensor cannot be used to measure the motor speed and the model is not validated. It can be seen that the validity range is limited by two lines (named D_1 and D_2 in the following). Several articles have defined analytic expressions of lines D_1 and D_2 using different methods [25,26]. Commonly, D_1 and D_2 are expressed using speed and torque ad standstill:

$$\begin{cases} T_{L_0} = -P\dfrac{\psi_{ref}^2}{R_R}\omega_0 \quad \text{noted } (D_2) \text{ inobservability line} \\ \text{and} \\ T_{L_0} = -P\dfrac{\psi_{ref}^2}{R_R}\left(\dfrac{\dfrac{R_R L_\sigma}{L_M R_s}+\dfrac{R_R}{R_s}}{1+\dfrac{R_R L_\sigma}{L_M R_s}+\dfrac{R_R}{R_s}}\right)\omega_0 \quad \text{named } (D_1). \end{cases} \tag{12}$$

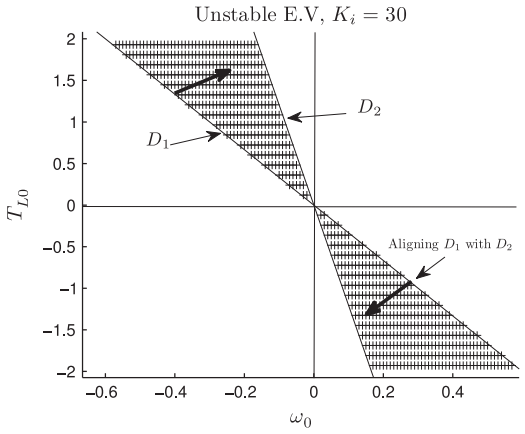

Fig. 12. UEV in the $\{\omega_0, T_{L0}\}$ plane, K_i=30, $G_s = G_r = 0$.

The line D_2 is defined by $\omega_{s0} = 0$ and reflects a physical property of the induction motor. The basic principle of speed estimation by observers is based on the information contained in the electromotive force (EMF) induced on the stator winding. At zero frequency the induced-EMF decrease and the rotor behavior cannot be deduced from stator measurements. The line D_2 corresponds to an intrinsic property of the motor which cannot be influenced by the observer design. However, the line D_1 depends on observer parameters and can be aligned with D_2 to obtain the largest validity range. This goal can be reached by modifying the model (3) through gains (G) and/or speed adaptation law design (5). The previous stability analysis calls into question the model selection proposed in Section 2.2 and according to the soft sensor development procedure shown in Fig. 1, a feedback must be done from step 4 to step 2.

5. Increasing the validity domain by a new model selection

5.1. Feedback gain design

5.1.1. Speed dependent gain

An optimal gain design can be obtain by aligning D_1 with D_2 (i.e. $D_1 = D_2$) and restricting the unstable region to D_2.

In [21], the authors have proposed the particular structure $G_s = \begin{bmatrix} g_{sd} & -g_{sq} \\ g_{sq} & g_{sd} \end{bmatrix}$, $G_r = \begin{bmatrix} g_{rd} & 0 \\ 0 & g_{rd} \end{bmatrix}$. By choosing the following parameters:

$$\begin{cases} g_{rd} = -R_s, \\ g_{sd} = kR_R/L_M, \\ g_{sq} = k\omega_0 \quad \text{with } k > 0, \end{cases} \tag{13}$$

the condition $D_1 = D_2$ can be reached. Theoretically, the sensor model is validated in all operating point except $\omega_s = 0$ if parameters are perfectly known. The reversal test in Fig. 13 shows the good behavior of the observer in the whole speed range. The frequency estimation error increases a little around zero speed but not long enough to cause a complete divergence of the estimation. Other solutions for speed dependant designs are proposed in [27].

5.1.2. Constant gain

In the solution (13), the parameter g_{sq} depends on the actual speed which unknown by definition. In practice, the actual speed is replaced by estimated one and the proof of stability used to find (13) seems to fail. Another solution is a feedback gain independent of ω_0 [28]. An appropriate structure is $G_s = 0$, $G_r = \begin{bmatrix} g_{rd} & -g_{rq} \\ g_{rq} & g_{rd} \end{bmatrix}$.

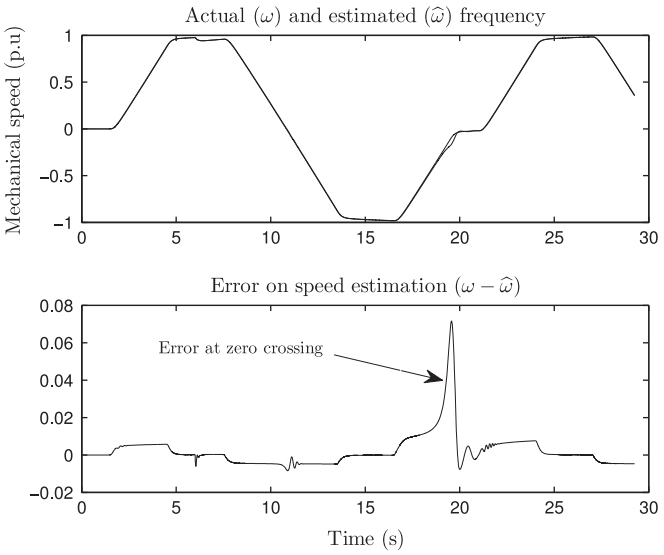

Fig. 13. Simulation results, reversal speed tests, G as (13), K_i=30.

A solution leading to $D_1 = D_2$ is

$$\begin{cases} g_{rq} = 0, \\ g_{rd} = -R_s. \end{cases} \tag{14}$$

For the inverse choice $G_r = 0$, $G_s = \begin{bmatrix} g_{sd} & -g_{sq} \\ g_{sq} & g_{sd} \end{bmatrix}$, an equivalent condition is

$$\begin{cases} g_{sq} = 0, \\ g_{sd} = -\dfrac{R_s}{L_\sigma}. \end{cases} \tag{15}$$

This design is similar to that proposed in [25] ($g_{sd} = -0.25R_s$). Simulation tests with nominal parameters provide the same results as those shown in Fig. 13. So, the unstable region is again reduced to D_2 but with a feedback gain G which is now independent of the real speed w.

In the remainder next subsection, the reduction of the unstable region to D_2 is performed by acting on the speed adaptation law.

5.2. Speed adaptation law design

In this section, a modified speed adaptation law is determined in order to reduce unstable regions to the line D_2. Several speed soft sensors use a modified adaptation law in order to stabilize state estimation in regenerating mode. The most general law is obtained by adding a complex number in estimated speed equation [22]:

$$\begin{cases} \dfrac{d}{dt}\underline{\widehat{i}}_s = -\left(\dfrac{1}{\tau_\sigma} + j\omega_s\right)\underline{\widehat{i}}_s + \dfrac{1}{L_\sigma}\left(\dfrac{1}{\tau_R} - j\widehat{\omega}\right)\underline{\widehat{\psi}}_R + \dfrac{1}{L_\sigma}\underline{u}_s, \\ \dfrac{d}{dt}\underline{\widehat{\psi}}_R = R_R\underline{\widehat{i}}_s - \left(\dfrac{1}{\tau_R} + j\widehat{\omega}_{s_l}\right)\underline{\widehat{\psi}}_R, \\ \dfrac{d}{dt}\widehat{\omega} = -K_i\Im\{e^{-j\phi}\underline{e}_i\underline{\widehat{\psi}}_R^*\}. \end{cases} \tag{16}$$

As in Section 5.1, the parameter ϕ reducing the unstable region to the inobservability line D_2 is sought.

The condition $D_1 = D_2$ is obtained by choosing

$$\phi_{opt} = \tan^{-1}\left(\frac{\omega_0 L_M}{R_R}\right). \tag{17}$$

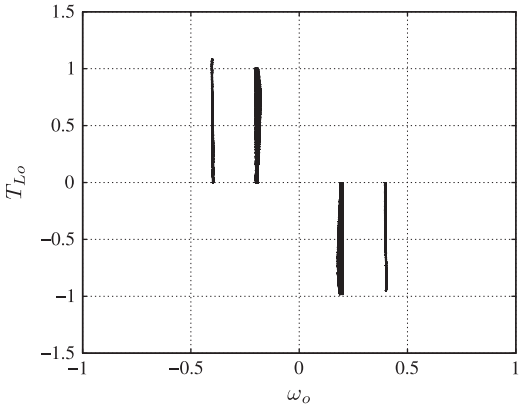

Fig. 14. Experimental results $\phi_{opt} = -\tan^{-1}(i_{sqo}/i_{sdo})$, tests in regenerating mode in the plan $\{\omega_0, T_{l0}\}$, K_i=1, K_p=0, $G_s = G_r = 0$. Rotor speed kept constant: $\omega_0 = -0.2$ and $\omega_0 = -0.4$ (quadrant 2), $\omega_0 = +0.2$ and $\omega_0 = +0.4$ (quadrant 4). Ramp of load torque from 0 to 1 (quadrant 2), from 0 to -1.5 (quadrant 4) during 100 s. Actual and estimated speeds are superimposed.

In low speed region, the angle (17) can be expressed using only measured signals:

$$\phi_{opt} \approx -\tan^{-1}\left(\frac{\omega_{sl0} L_M}{R_R}\right), \quad \text{i.e.} \tag{18}$$

$$\tan(\phi_{opt}) = -\frac{i_{sqo}}{i_{sdo}}. \tag{19}$$

Finally, the optimal solution is

$$\phi_{opt} = -\tan^{-1}\left(\frac{i_{sqo}}{i_{sdo}}\right). \tag{20}$$

Experimental results corresponding to modified model (16) are shown in Fig. 14. In comparison with Fig. 11, the model is validated in regenerating mode.

6. Conclusion

In this paper, we have presented the complete design of a soft sensor for speed measurement of induction motor. In one hand, the step of validation has been investigated with a stability analysis using automatic theory. One the other hand, the proposed stability criterion was used to determine the validated model in the whole operating range of the sensor. From our point of view, this approach offers new tools when the validation step leads to a necessary modification of the model. It can be generalized and applied to other types of sensors in the field of electrical engineering. Model validation by control theory is particularly suitable when external disturbances affect the operation of the sensor. In the case of control of electric motors, the temperature can vary several parameters, in particular the resistance of the windings. This can lead to a malfunction of the soft sensor and a new validation study should be conducted. In this case, the state representation used in this paper is particularly suitable and can lead to a viable solution. This new step is the subject of new works in our laboratory.

References

[1] Abdelli R, Rekioua D, Rekioua T. Performances improvements and torque ripple minimization for VSI fed induction machine with direct control torque. ISA Transactions 2011;50.
[2] Achour AY, Mendil B, Bacha S, Munteanu I. Passivity-based current controller design for a permanent-magnet synchronous motor. ISA Transactions 2009;48.
[3] Zhang B, Pi Y, Luo Y. Fractional order sliding-mode control based on parameters auto-tuning for velocity control of permanent magnet synchronous motor. ISA Transactions 2012;51.
[4] Bogaerts PH, Vande Wouwer A. Software sensors for bioprocesses. ISA Transactions 2003;42(October (4)):547–58.
[5] Escobar a RF, Astorga-Zaragoza a CM, Tellez-Anguiano c AC, Juarez-Romero b D, Hernandezb JA, Guerrero-Ramirez GV. Sensor fault detection and isolation via high-gain observers: application to a double-pipe heat exchanger. ISA Transactions 2011;50:480–6.
[6] Vijaya Raghavana SR, Radhakrishnan a TK, Srinivasan K. Soft sensor based composition estimation and controller design for an ideal reactive distillation column. ISA Transactions 2011;50:61–70.
[7] Kubota H, Matsuse K. DSP-based speed adaptive flux observer of induction motor. IEEE Transactions on Industrial Applications 1993;29(March/April (2)):344–8.
[8] Karimia HR, Babazadehb A. Modeling and output tracking of transverse flux permanent magnet machines using high gain observer and RBF Neural network. ISA Transactions 2005;44:445–6.
[9] Hinkkanen M, Harnefors M, Luomi J. Reduced-order flux observers with stator-resistance adaptation for speed-sensorless induction motor drives. IEEE Transactions on Power Electronics 2010;25(April (5)).
[10] Yang G, Chin T. Adaptive-speed identification Scheme for a vector-controlled speedsensorless inverter-induction motor drive. IEEE Transactions on Industrial Applications 1993;29(July/August (4)):820–5.
[11] Madadi-Kojabadi G. Simulation and experimental studies of model reference adaptive system for sensorless induction motor drive. Simulation Modelling Practice and Theory 2005;13(6):5–11.
[12] Orlowska-Kowalska T, Dybkowski M. Stator-current-based MRAS estimator for a wide range speed-sensorless induction-motor drive. IEEE Transactions on Industrial Electronics 2010;57(April (4)).
[13] Fortuna L, Graziani S, Rizzo A. Soft sensors for monitoring & control of industrial processes (Advances in industrial control). Springer; 2006.
[14] Trigeassou JC, Poinot T, Moreau S. A methodology for estimation of physical parameters. System Analysis Modelling Simulation 2003;43:925–43.
[15] Vas P. Sensorless vector and direct torque control. Oxford University Press; 1998.
[16] Koubaa Y. Recursive identification of induction motor parameters. Simulation Modelling Practice and Theory 2004;12(5).
[17] Ljung L. System identification – theory for the user. Prentice Hall; 1987.
[18] Marquardt WD. An algorithm for least squares estimation of nonlinear parameters. Journal of the Society for Industrial and Applied Mathematics 1963;11(June):431–41.
[19] Tajima H, Guidi G. Consideration about problems and solutions of speed estimation method and parameter tuning for speed-sensorless vector control of induction motor drives. IEEE Transactions on Industrial Applications 2002;38(5).
[20] Beguenane R, Ouhrouche MA, Trzynadlowski AM. A new scheme for sensorless induction motor control drives operating in low speed region. Mathematics and Computers in Simulation 2006;71(2).
[21] Suwankawin S, Sangwongwanich S. Design strategy of an adaptive full-observer for speed-sensorless induction-motor drives-tracking performance and stabilization. IEEE Transactions on Industrial Electronics 2006;53(1).
[22] Hinkkanen M. Stabilization of regenerating-mode operation in sensorless induction motor drives by full-order flux observer design. IEEE Transactions on Industrial Electronics 2004;51(6).
[23] Sangwongwanich S, Suwankawin S, Po-ngam S, Koonlaboon S. A unified speed estimation design framework for sensorless ac motor drives based on positive-real property. In: Conference record, Power conversion conference Nagoya; 2007.
[24] Etien E, Chaigne C, Bensiali N. On the stability of full adaptive observer for induction motor in regenerating mode. IEEE Transactions on Industrial Electronics 2010;57(5).
[25] Suwankawin S, Sangwongwanich S. A speed-sensorless in drive with decoupling control and stability analysis of speed estimation. IEEE Transactions on Industrial Electronics 2002;49(April (2)):444–55.
[26] Rashed M, Stronach F, Vas P. A stable MRAS-based sensorless vector control induction motor drive at low speeds, In: Conference record IEEE IEMDC; 2003.
[27] Kubota G, Sato L, Tamura Y, Matsume K, Ohta H, Hori Y. Stable operation of adaptive observer based sensorless induction motor drives in regenerating mode at low speeds. In: Conference record IAS annual meeting; 2001.
[28] Bouhenna A, Chaigne C, Bensiali N, Etien E, Champenois G. Design of speed adaptation law in sensorless control of induction motor in regenerating mode. Simulation Modelling Practice and Theory 2007;15(7).